Robust Attitude Control for Reusable Launch Vehicles Based on Fractional Calculus and Pigeon-inspired Optimization

Qiang Xue and Haibin Duan, *Senior Member, IEEE*

***Abstract*—In this paper, a robust attitude control system based on fractional order sliding mode control and dynamic inversion approach is presented for the reusable launch vehicle (RLV) during the reentry phase. By introducing the fractional order sliding surface to replace the integer order one, we design robust outer loop controller to compensate the error introduced by inner loop controller designed by dynamic inversion approach. To take the uncertainties of aerodynamic parameters into account, stochastic robustness design approach based on the Monte Carlo simulation and Pigeon-inspired optimization is established to increase the robustness of the controller. Some simulation results are given out which indicate the reliability and effectiveness of the attitude control system.**

***Index Terms*—Attitude control, fractional calculus, pigeon-inspired optimization, reusable launch vehicle (RLV), sliding mode control.**

I. Introduction

With the necessity of the development of reusable space transportation system as well as the hypersonic weapons with high penetration ability and kill efficiency, reusable launch vehicle (RLV) technology becomes a hot research field all over the world [1]. Unpowered gliding reentry vehicle is one of the implementations which have the aerodynamic configuration with high lift-to-drag ratio (L/D). During the reentry phase, the flight envelope ranges from over Mach 20 to Mach 1 and altitude ranges from 100 km to 20 km [2]. When reusable launch vehicle maneuvers in the so called near space, the flow field around the vehicle would present the hypersonic flow dynamic characteristics, such as viscous interference, thin shock layer, low density effect and so on [3]. Thus, complex coupling between state variables and control variables, high nonlinear terms and strongly time varying characteristics take into the dynamics of reentry vehicles.

Facing with these challenges, the guidance and control technology becomes one of the key issues in the development process of reusable launch vehicles [4]. Guidance subsystem leads the vehicle to steer the reference trajectory or predict trajectory onboard, while control subsystem stabilizes the attitude and takes attitude maneuver to track guidance commands. By introducing advanced control theories such as adaptive control theory, dynamic inversion approach and sliding mode control, the robustness and effectiveness of the flight control systems were obviously improved [4], compared with some classical design techniques such as gain-scheduling methods. Recently, the dynamic inversion technique was applied into the flight control law design process, especially in reentry flight control and high angle of attack maneuver, demonstrated several advantages [5]. However, it required a precise model to avoid the error introduced by inversion, which might strongly influence the control qualities. The saturation of actuators is also an additional serious problem which should be avoided. However, another nonlinear control method named sliding mode control approach as a robust control technique has been widely applied in the flight control law design which could tolerate the uncertainties of models and disturbance. Unfortunately, there are some problems when applying the sliding mode method directly. For example, the order of the sliding mode method would be high when the controlled model is complex, which might make the algorithm difficult to be employed.

Fractional calculus theory, which is about integration and differential with non-integer orders, has a rapid development with an increasing attention since hundred years ago. More and more attention focuses on the application of fractional calculus in the modeling and control in engineering viewpoint [6]. Some designs based on fractional calculus for flight control system also present the possibility of the application and the advantages compared with traditional integer control approach [7]. In general, the fractional order of integral or derivation is more flexible and widely used than the integer order. To introduce the fractional calculus in these control method, the performance of closed-loop systems could probably be improved and control inputs could be reduced. Therefore, applying fractional calculus in reusable launch vehicle attitude control would be a beneficial trial.

In fact, the uncertainties of aerodynamic coefficients are also necessary to be taken into consideration in the process of control law design. It demands that the control system could tolerate these uncertainties of the coefficients and endure any dispersion. In order to improve the robustness of control system, the stochastic robustness method based on Pigeon-inspired optimization is introduced. By this procedure, the optimal parameters of the controller have been obtained and the controller is optimal in terms of stochastic robustness. Therefore, a combined and robust control structure based on stochastic robustness design method is established to overcome these challenges mentioned previously. In this

Manuscript received August 30, 2015; accepted November 17, 2015. This work was supported by National Natural Science Foundation of China (61425008, 61333004, 61273054), Top-Notch Young Talents Program of China, and Aeronautical Foundation of China (2015ZA51013). Recommended by Associate Editor YangQuan Chen.

Citation: Q. Xue and H. B. Duan, "Robust attitude control for reusable launch vehicles based on fractional calculus and pigeon-inspired optimization," *IEEE/CAA Journal of Automatic Sinica*, vol. 4, no. 1, pp. 89−97, Jan. 2017.

Q. Xue and H. B. Duan are with Bio-inspired Autonomous Flight Systems (BAFS) Research Group, the Science and Technology on Aircraft Control Laboratory, School of Automation Science and Electrical Engineering, Beihang University (BUAA), Beijing 100083, China (e-mail: xueqiang@buaa.edu.cn; hbduan@buaa.edu.cn).

Color versions of one or more of the figures in this paper are available online at http://ieeexplore.ieee.org.

Digital Object Identifier 10.1109/JAS.2017.7510334

structure, the dynamic inversion is applied to design the inner loop controller, while the fractional sliding mode approach is applied to design the outer loop controller. The fractional sliding mode approach could weak the integral action and decrease the control input. It could also smooth the time history of controlled variables. The stochastic robustness method based on PIO algorithm allows us to obtain the optimal controller in terms of stochastic robustness. The organization of this paper is as follows. In Section II, the description of the reusable launch vehicle model is presented. In Section III, the control system including control law and control allocation algorithm is established. The control law is based on fractional sliding mode control (FSMC) and dynamic inversion (DI) approach, and the control allocation algorithm is a commonly used algorithm. In Section IV, the stochastic robustness design method based on a new swarm intelligent algorithm, i.e., pigeon-inspired optimization is introduced, based on which we design stochastic robustness optimal controller. In Section V, we give the design examples and simulation results to demonstrate the robustness and effectiveness of the control system, and the influence of different fractional orders of FSMC to the closed-loop system is discussed.

II. Attitude Control Problem

A. Mathematical Model of Attitude Dynamics

The mathematical equations of reentry dynamics consist of the translational motion associated with flight path variables and the rotational motion associated with attitude angles which used to be aerodynamic angles during the reentry phase. The three-degree-of-freedom model of unpowered reentry attitude dynamics is given out as follows [8]:

$$\begin{aligned}\dot{\alpha} &= q - (p\cos\alpha + r\sin\alpha)\tan\beta \ - \dot{\gamma}\cos\mu/\cos\beta \\ &\quad - \dot{\chi}\cos\gamma\sin\mu/\cos\beta \end{aligned} \tag{1}$$

$$\dot{\beta} = p\sin\alpha - r\cos\alpha - \dot{\gamma}\sin\mu + \dot{\chi}\cos\gamma\cos\mu \tag{2}$$

$$\begin{aligned}\dot{\mu} &= p\cos\alpha/\cos\beta + r\sin\alpha/\cos\beta \\ &\quad + \dot{\chi}(\sin\gamma + \tan\beta\sin\mu\cos\gamma) + \dot{\gamma}\tan\beta\cos\mu \end{aligned} \tag{3}$$

where α is the angle of attack, β is the angle of sideslip, μ is the bank angle, γ is the flight-path angle, and χ is the airspeed heading angle.

The rotational dynamic equation is as follows:

$$\begin{aligned}\dot{p} &= I_{lp}M_x + I_{np}M_z + \frac{(I_y - I_z)I_z - I_{xz}^2}{I_xI_z - I_{xz}^2}qr \\ &\quad + \frac{(I_x - I_y + I_z)I_{xz}}{I_xI_z - I_{xz}^2}pq \end{aligned} \tag{4}$$

$$\dot{q} = I_{mq}M_y + \frac{I_z - I_x}{I_y}pr - \frac{I_{xz}}{I_y}(p^2 - r^2) \tag{5}$$

$$\begin{aligned}\dot{r} &= I_{lr}M_x + I_{nr}M_z + \frac{I_x(I_x - I_y) + I_{xz}^2}{I_xI_z - I_{xz}^2}pq \\ &\quad - \frac{(I_x - I_y + I_z)I_{xz}}{I_xI_z - I_{xz}^2}qr \end{aligned} \tag{6}$$

$$\begin{aligned} I_{lp} &= \frac{I_z}{I_xI_z - I_{xz}^2}, \quad I_{np} = \frac{I_{xz}}{I_xI_z - I_{xz}^2}, \quad I_{mq} = \frac{1}{I_y} \\ I_{lr} &= \frac{I_{xz}}{I_xI_z - I_{xz}^2}, \quad I_{nr} = \frac{I_x}{I_xI_z - I_{xz}^2} \end{aligned} \tag{7}$$

where $\vec{w} = (p, q, r)^T$are the roll rate, the pitch rate and the yaw rate, $\vec{M} = (M_x, M_y, M_z)$are the moments acting on the vehicle, consisting of aerodynamic trim moments and control torques generated by aerodynamic surfaces and reaction control systems.

$$I = \begin{bmatrix} I_x & -I_{xy} & -I_{xz} \\ -I_{xy} & I_y & -I_{yz} \\ -I_{xz} & -I_{yz} & I_z \end{bmatrix}$$

which is the inertia matrix.

B. Improved Aerodynamic Model of RLV

The aerodynamic moments generated by the aerodynamic control surfaces could be calculated by the following standard formulation:

$$\bar{L} = C_{l,total}q_{bar}SL_{ref} \tag{8}$$

$$M = C_{m,total}q_{bar}SL_{ref} \tag{9}$$

$$N = C_{n,total}q_{bar}SL_{ref} \tag{10}$$

where $\bar{L}$ is the roll aerodynamic moment, M is the pitch aerodynamic moment, N is the yaw aerodynamic moment, q_{bar} is the dynamic pressure, S is the reference area, L_{ref} is the reference length, $C_{l,total}$ is the non-dimensional roll moment coefficient, $C_{m,total}$ it he non-dimensional pitch moment coefficient, and $C_{n,total}$ is the non-dimensional yaw moment coefficient.

The reusable launch vehicle used in this study is configured with several aerodynamic surfaces: four body flaps placed at the tail, two elevons and one rudder. In order to simplify the relationship between the motion channel and the control surface deflection, nominal control surfaces are introduced to replace the actual aerodynamic surfaces with the transformational matrix as follows [9]:

$$\begin{bmatrix} 0 & 0 & 0 & 0 & 0.5 & -0.5 & 0 \\ 0 & 0 & 0 & 0 & 0.5 & 0.5 & 0 \\ 0 & 0 & 0 & 0 & 0 & 0 & 1 \\ 0.5 & 0.5 & 0 & 0 & 0 & 0 & 0 \\ 0 & 0 & 0.5 & 0.5 & 0 & 0 & 0 \\ 0.5 & -0.5 & 0.5 & -0.5 & 0 & 0 & 0 \end{bmatrix} \begin{bmatrix} \delta_{LLBP} \\ \delta_{LRBP} \\ \delta_{ULBP} \\ \delta_{URBP} \\ \delta_{WL} \\ \delta_{WR} \\ \delta_r \end{bmatrix} = \begin{bmatrix} \delta_a \\ \delta_e \\ \delta_r \\ \delta_{f+} \\ \delta_{f-} \\ \delta_{\Delta f} \end{bmatrix}. \tag{11}$$

As for our specific developed reentry vehicle, the original formulations of the moment coefficients are shown in (12)−(14) [10].

$$\begin{aligned} C_{l,total} &= C_{l\beta,basic}\beta + \Delta C_{l,BF} + \Delta C_{l,rudder} \\ &\quad + \Delta C_{l.Elevon} + \Delta C_{l\beta,GE}\beta + \Delta C_{l\beta,LG}\beta \\ &\quad + \Delta C_{lp}\frac{pb}{2V} + \Delta C_{lr}\frac{rb}{2V} \end{aligned} \tag{12}$$

$$\begin{aligned} C_{m,total} &= C_{m,basic} + \Delta C_{m,BF} + \Delta C_{m,Elevon} \\ &\quad + \Delta C_{m,rudder} + \Delta C_{m,GE} + \Delta C_{m,LG} + \Delta C_{mq}\frac{qc}{2V} \end{aligned} \tag{13}$$

$$\begin{aligned} C_{n,total} &= C_{n\beta,basic}\beta + \Delta C_{n,BF} + \Delta C_{n,elevon} \\ &\quad + \Delta C_{n,rudder} + \Delta C_{n\beta,GE}\beta + \Delta C_{n\beta,LG}\beta \\ &\quad + \Delta C_{np}\frac{pb}{2V} + \Delta C_{nr}\frac{pr}{2V}. \end{aligned} \tag{14}$$

According to the relations between the actual surfaces and nominal surfaces, and converting the aerodynamic coefficients to the aerodynamic derivatives by $C_{i,j} = \Delta C_{i,j}/\Delta\delta_j$, the

developed formulation of the moment coefficients could be obtained as follows:

$$C_{l,total} = C_{l\beta,basic}\beta + C_{l\delta_a}\delta_a + C_{l\delta_r}\delta_r + C_{l\delta_{\Delta f}}\delta_{\Delta f} + C_{lp}\frac{pb}{2V} + C_{lr}\frac{rb}{2V} \quad (15)$$

$$C_{m,total} = C_{m,basic} + C_{m\delta_e}\delta_e + C_{m\delta_{f+}}\delta_{f+} + C_{m\delta_{f-}}\delta_{f-} + \Delta C_{mq}\frac{qc}{2V} \quad (16)$$

$$C_{n,total} = C_{n\beta,basic}\beta + C_{n\delta_a}\delta_a + C_{n\delta_r}\delta_r + C_{np}\frac{pb}{2V} + C_{nr}\frac{pr}{2V} \quad (17)$$

where $\delta = [\delta_a\ \delta_e\ \delta_r\ \delta_{f+}\ \delta_{f-}\ \delta_{\Delta f}]$ is deflection vector of the aerodynamic control surfaces ranking as the aileron, elevator, rudder, body flap positive deflection, body flap negative deflection and body flap differential deflection.

These aerodynamic coefficients and derivatives mentioned above could be obtained from the complete set of the coefficient and derivative lookup table vs Mach and AOA using interpolation algorithm.

C. Attitude Control Strategy

In the design process of reentry flight attitude control law, adequate engineering practices present the feasibility and effectiveness of the application of time-scale separation principle to deal with the flight state variables [5], [11]. The aerodynamic angles including angle of attack and slip slide angle and bank angle are regarded as the slow variables of the outer loop, while the angle rates around body axis are regarded as the fast variables of the inner loop. Dual loop control framework could be designed for the inner loop and outer loop: the function of inner loop controller is to track the angular rate commands generated by the outer loop, while the outer loop controller operates to control aerodynamic commands.

In this study, dynamic inversion approach is chosen to design the dual loop controller and obtain three channel decoupling model of aerodynamic angles, and sliding mode technique improved by fractional calculus is used to design to provide the desired time-scale separation [2]. Thus, when guidance commands are given out from guidance subsystem, the required total control torque would be generated by the control law. The control torque allocation algorithm presents the mapping relation between the control torque and control surface deflections. By combining control law and control torque allocation, the complete attitude control system is established. The framework of the whole system is shown in Fig. 1.

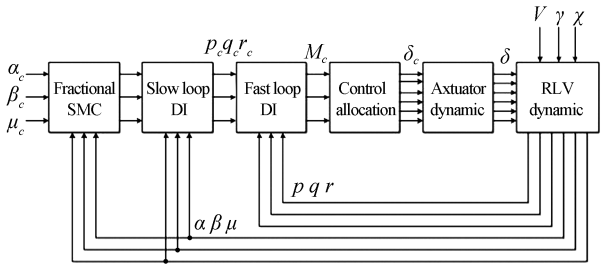

Fig. 1. The diagram of control system.

III. Implementation of the Attitude Control System

A. Fractional Calculus and Approximate Form of Fractional Calculus Operator

The Caputo's definition of the fractional derivative of order α with respect to variable t and initial point at $t = 0$ is as follows [12]:

$${}_0D_t^{\alpha} f(t) = \frac{1}{\Gamma(1-\delta)}\int_0^t \frac{f^{(m+1)}(\tau)}{(t-\tau)^{\delta}}d\tau \quad (\alpha = m+\delta;\ m \in \mathbb{Z};\ 0 < \delta \le 1) \quad (18)$$

where $\Gamma(\cdot)$ is the gamma function [12]:

$$\Gamma(\xi) = \int_0^{\infty} e^{-m} m^{\xi-1} dm. \quad (19)$$

The Grunwald-Letnikov's fractional derivative of order m is defined as follows:

$${}_aD_t^m f(t) = \lim_{h\to\infty} h^{-m} \sum_{j=0}^{\frac{t-m}{h}} (-1)^j \binom{m}{j} f(t-jh) \quad (20)$$

where h is the step size, a is the lower limit of integral and t is the upper limit of integral. The Laplace transform of fractional derivative is given as follows:

$$L\{{}_0D_t^{\alpha} f(t)\} = s^{\alpha}F(s) - [{}_0D_t^{\alpha-1} f(t)]_{t=0} \quad (21)$$

$$L\{{}_0D_t^{-\alpha} f(t)\} = s^{-\alpha}F(s). \quad (22)$$

One of the digital implement of fractional derivative is using the discrete filter to approximate it which can be easily applied in engineering practice [13]. In this study, the directly discretization method is conducted to obtain the equivalent discrete filter. Firstly, apply Tustin mapping function to transform the fractional derivative from S domain to Z domain:

$$s^{\pm\alpha} = (w(z^{-1}))^{\pm\alpha} \quad (23)$$

where $w(\cdot)$ is the Tustin mapping function as follows:

$$w(z^{-1}) = \frac{2}{T}\frac{1-z^{-1}}{1+z^{-1}}. \quad (24)$$

Then the CFE (continued fraction expansion) method is used to obtain the rationalization result of the fractional derivative model in Z domain. The whole procedure of Tustin with CFE method is as follows [14]:

$$D_E^{\pm\alpha}(z) = \left(\frac{1}{T}\right)^{\pm\alpha} CFE\{(1-z^{-1})^{\pm\alpha}\}_{p,q} = \left(\frac{1}{T}\right)^{\pm\alpha} \frac{P_p(z^{-1})}{Q_q(z^{-1})} \quad (25)$$

B. Dual Loop Control Law Designed by Nonlinear Dynamic Inversion Approach

According to time-scale separation principle, control law could be designed separately for the fast loop variables and the slow loop variables. It is assumed that the dynamic of fast loop is so fast that does not affect the responses of slow loop.

For the fast loop, a first-order desired dynamic could be chosen as follows [2], [5]:

$$\begin{bmatrix}\dot{p}\\ \dot{q}\\ \dot{r}\end{bmatrix}_{des} = K_w\left(\begin{bmatrix}p_c\\ q_c\\ r_c\end{bmatrix} - \begin{bmatrix}p\\ q\\ r\end{bmatrix}\right). \quad (26)$$

Combined with the rotational dynamic (4)−(6), the required total torque could be calculated as follows:

$$\begin{bmatrix} M_x \\ M_y \\ M_z \end{bmatrix} = \begin{bmatrix} I_{lp} & 0 & I_{np} \\ 0 & I_{mq} & 0 \\ I_{lr} & 0 & I_{nr} \end{bmatrix}^{-1} \times \left(\begin{bmatrix} \dot{p} \\ \dot{q} \\ \dot{r} \end{bmatrix}_{des} - \begin{bmatrix} \frac{(I_y-I_z)I_z-I_{xz}^2}{I_xI_z-I_{xz}^2}qr + \frac{(I_x-I_y+I_z)I_{xz}}{I_xI_z-I_{xz}^2}pq \\ \frac{I_z-I_x}{I_y}pr - \frac{I_{xz}}{I_y}(p^2-r^2) \\ \frac{I_x(I_x-I_y)+I_{xz}^2}{I_xI_z-I_{xz}^2}pq - \frac{(I_x-I_y+I_z)I_{xz}}{I_xI_z-I_{xz}^2}qr \end{bmatrix} \right). \tag{27}$$

Subtracting the basic aerodynamic moments and damping aerodynamic moments from the total required torque, the required control torque is obtained as in (28).

$$M_c = M - M_a. \tag{28}$$

The fast loop control law allows the angular rates to be able to track the angular rate commands, while the angular rate commands are generated by the slow loop. The characteristics of fast loop dynamic such as the bandwidth depend on parameter K_w.

For the slow loop, the rotational motion equations about aerodynamic angles could be rearranged in vector form as follows [2]:

$$\begin{aligned} \begin{bmatrix} \dot{\alpha} \\ \dot{\beta} \\ \dot{\mu} \end{bmatrix} &= \begin{bmatrix} -\cos\alpha\tan\beta & 1 & -\sin\alpha\tan\beta \\ \sin\alpha & 0 & -\cos\alpha \\ \cos\alpha/\cos\beta & 0 & \sin\alpha/\cos\beta \end{bmatrix} \begin{bmatrix} p \\ q \\ r \end{bmatrix} + \begin{bmatrix} v_\alpha \\ v_\beta \\ v_\mu \end{bmatrix} \\ &= L \begin{bmatrix} p \\ q \\ r \end{bmatrix} + \begin{bmatrix} v_\alpha \\ v_\beta \\ v_\mu \end{bmatrix} \end{aligned} \tag{29}$$

$$\begin{bmatrix} v_\alpha \\ v_\beta \\ v_\mu \end{bmatrix} = \begin{bmatrix} -1/\cos\beta(\dot{\gamma}\cos\mu + \dot{\chi}\cos\gamma\sin\mu) \\ \dot{\chi}\cos\mu\cos\gamma - \dot{\gamma}\sin\mu \\ \dot{\gamma}\cos\mu\tan\beta + \dot{\chi}(\cos\gamma\sin\mu\tan\beta + \sin\gamma) \end{bmatrix}. \tag{30}$$

When β satisfies the inequality $\beta \neq \pm 90^\circ$, matrix L is invertible, while in the reentry flight phase this condition is always satisfied. Thus, assuming v is the virtual control input, the fast loop input, i.e., angular rate commands could be obtained as follows:

$$\begin{bmatrix} p \\ q \\ r \end{bmatrix}_c = \begin{bmatrix} 0 & \sin\alpha & \cos\alpha\cos\beta \\ 1 & 0 & \sin\beta \\ 0 & -\cos\alpha & \sin\alpha\cos\beta \end{bmatrix} \left(v - \begin{bmatrix} v_\alpha \\ v_\beta \\ v_\mu \end{bmatrix} \right). \tag{31}$$

According to time-scale separation principle, the fast loop dynamic is so fast compared with the dynamic of the slow loop which allows us to suppose that the angular rate is equal to the angular rate command.

By introducing the dual loop control law, the three channels have been decoupled and a linear system is obtained as follows:

$$\begin{bmatrix} \dot{\alpha} \\ \dot{\beta} \\ \dot{\mu} \end{bmatrix} = v. \tag{32}$$

C. Sliding Mode Control Design Based on Fractional Calculus

For the decoupling linear system about three aerodynamic angle channels, a sliding mode control law based on fractional calculus is designed to obtain the virtual control input v of dual loop dynamic inversion law and compensating the error generated by dynamic inversion approach.

First, define the attitude error as in (33), and choose the fractional sliding surface function as in (34).

$$e = [\alpha_c - \alpha \quad \beta_c - \beta \quad \mu_c - \mu]^T \tag{33}$$

$$S = e + K \cdot {}_0D_t^{\lambda} e. \tag{34}$$

The fractional exponential reaching law is chosen as follows:

$${}_0D_t^{\eta} S = -\kappa S - \sigma\,\mathrm{sign}(S) \tag{35}$$

where the parameters above are defined as:

$$\kappa = \mathrm{diag}\{\kappa_\alpha, \kappa_\beta, \kappa_\mu\}, \quad \sigma = \mathrm{diag}\{\sigma_\alpha, \sigma_\beta, \sigma_\mu\}$$
$$\kappa_\alpha, \kappa_\beta, \kappa_\mu > 0; \quad \sigma_\alpha, \sigma_\beta, \sigma_\mu > 0.$$

Combine (34) and (35), the virtual control input v could be obtained.

$$\begin{aligned} \dot{S} &= \frac{d}{dt}(e + K \cdot {}_0D_t^{\lambda} e) \\ &= \dot{e} + K \cdot {}_0D_t^{\lambda+1} e = {}_0D_t^{1-\eta}(-\kappa S - \sigma\,\mathrm{sign}(S)) \end{aligned} \tag{36}$$

$$\begin{aligned} v &= \begin{bmatrix} \dot{\alpha} \\ \dot{\beta} \\ \dot{\mu} \end{bmatrix} \\ &= \begin{bmatrix} \dot{\alpha}_c + k_{\alpha 0} D_t^{\lambda+1}(\alpha_c - \alpha) + {}_0D_t^{1-\eta}[\kappa_\alpha S_\alpha + \sigma_\alpha\,\mathrm{sign}(S_\alpha)] \\ \dot{\beta}_c + k_{\beta 0} D_t^{\lambda+1}(\beta_c - \beta) + {}_0D_t^{1-\eta}[\kappa_\beta S_\beta + \sigma_\beta\,\mathrm{sign}(S_\beta)] \\ \dot{\mu}_c + k_{\mu 0} D_t^{\lambda+1}(\mu_c - \mu) + {}_0D_t^{1-\eta}[\kappa_\mu S_\mu + \sigma_\mu\,\mathrm{sign}(S_\mu)] \end{bmatrix} \end{aligned} \tag{37}$$

where $S = [S_\alpha\, S_\beta\, S_\mu]^T$. In the next, D^λ is used to replace the description ${}_0D_t^{\lambda}$.

D. Control Allocation Algorithm

The control law designed above generates the required control torque command to steer the guidance commands, while the control torque is generated by vehicle's control surfaces. For reentry vehicles, they always configure with hybrid control surfaces including aerodynamic control surfaces and reaction control systems (RCS). During early reentry phase, both aerodynamic control surfaces and RCS are operated, while pure aerodynamic control surfaces are operated during final reentry phase. In this study, the terminal of reentry phase is focused on and pure aerodynamic control surfaces are used to generate all the control torques:

$$\begin{bmatrix} M_{cx} \\ M_{cy} \\ M_{cz} \end{bmatrix} = qSL_{ref}C \begin{bmatrix} \delta_a \\ \delta_e \\ \delta_r \\ \delta_{f+} \\ \delta_{f-} \\ \delta_{\Delta f} \end{bmatrix} = qSL_{ref}C\delta \tag{38}$$

where C is the control matrix with aerodynamic derivatives:

$$C = \begin{bmatrix} C_{l\delta_a} & 0 & C_{l\delta_r} & 0 & 0 & C_{l\delta_{\Delta f}} \\ 0 & C_{m\delta_e} & 0 & C_{m\delta_{f+}} & C_{m\delta_{f-}} & 0 \\ C_{n\delta_a} & 0 & C_{n\delta_r} & 0 & 0 & 0 \end{bmatrix} \tag{39}$$

$$\operatorname{rank}(C) = 3. \tag{40}$$

The reference control allocation strategy is chosen in [8], [15]:

$$\delta_{c,rtd} = Q^{-1}C^T[CQ^{-1}C^T]^{-1}\frac{M_c}{qSL_{ref}}. \tag{41}$$

If the rated deflection of aerodynamic surfaces is saturated, the saturated value is chosen to be the deflection command, although it is important to try to avoid these conditions.

IV. Principles of PIO Algorithm and Stochastic Robustness Design

A. PIO Algorithm Description and Principles

PIO algorithm, firstly proposed by Duan and Qiao, is a swarm intelligence algorithm inspired by the behavior of homing pigeons [16]. As presented in [16], homing pigeons are considered to go home by three homing tools: magnetic field, sun and landmarks. The homing behaviors depending on different homing tools are mapping to the update formulations in this new evolution algorithm. The detailed description of PIO is as follows [16]:

Individual in the pigeon swarm is initialized with initial velocity V_i and the initial position X_i in D-dimension research space randomly, while the position is the vector formed by parameters to be optimized and the velocity is the vector to update the position vector. Each individual is related to a value named the fitness value which is the cost function and always depends on the position of the individual. The evolution algorithm is to find the best position which has the maximum or minimum cost function. Two operators, map and compass operator and landmark operator, are introduced to model the two homing behaviors as mentioned early. At the early moment, pigeons are supposed to adjust their direction to the destination by the map shaped in their brains and compass. Thus, in this map and compass operator, the pigeon is trend to the global best position by the update formulations as follows:

$$V_i(t) = V_i(t-1)\cdot e^{-Rt} + \operatorname{rand}\cdot(X_{g,best} - X_i(t-1)) \tag{42}$$

$$X_i(t) = X_i(t-1) + V_i(t) \tag{43}$$

where R is defined as the map and compass factor, $X_{g,best}$ denotes the global best position among all individual in current iteration, rand signifies a random number.

With pigeons approaching to the destination, they switch their homing tool from map and compass to landmark, which means the landmark operator starts. In the landmark operator, pigeons are halved in every iteration generation. The pigeons which are familiar to the landmark fly straight to the destination, while others are supposed to follow the ones which are familiar to the landmark. In this model, the destination is regarded as the center of all pigeons in current iteration generation and can be calculated by weighted average of the position, the formulation is as follows:

$$X_c(t) = \frac{\sum\limits_{N_p} X_k(t)\cdot \operatorname{fitness}(X_k(t))}{\sum\limits_{N_p}\operatorname{fitness}(X_k(t))}. \tag{44}$$

In addition, the number of pigeons would be updated as follows:

$$N_p(t) = \frac{N_p(t-1)}{2}. \tag{45}$$

In this operator, the update formulation of the position of pigeons can be written as follows:

$$X_i(t) = X_i(t-1) + \operatorname{rand}\cdot(X_c(t) - X_i(t-1)). \tag{46}$$

Several papers indicate the effectiveness and robustness to solve some optimization problems or converted optimization problem, such as target detection, air robot path planning problem, UAVs formation cooperative control problem and so on [16]−[19]. In this study, PIO algorithm is selected to design parameters of the controller using stochastic robustness design method.

B. Stochastic Robustness Design Method

Due to the difficulties of the application of classical robust control theoretics in engineering practice, R.F. Stengel *et al.* introduced the concept of stochastic robustness and established a new robust control design method named stochastic robustness analysis and design (SRAD) in 1990s, which has been widely applied in engineering practice especially in flight control area in the past years [20]−[22].

In Stengel's theoretic, for linear time invariant (LTI) system, suppose that there are uncertain parameters $v \in \mathcal{Q}$, the instability probability can be defined as follows [23]:

$$P_{\text{instability}} = 1 - \int_{v\in\mathcal{Q}, g(v)\le 0} f(x)dx \tag{47}$$

where $g(v) = [\sigma_1(v)\sigma_2(v)\cdots\sigma_n(v)]^T$ is the vector formed by the real parts of the eigenvalues of closed-loop system, $f[g(v)]$ is the combined probability density distribution function. In practical application, the instability probability can be calculated by sample frequency calculation instead of the integral calculation, i.e.,

$$\int_{v\in\mathcal{Q}, g(v)\le 0} f(x)dx = \lim_{N\to\infty}\left.\frac{M[g_{\max}(v)\le 0]}{N}\right|_{v\in\mathcal{Q}} \tag{48}$$

where $g_{\max}(v) = \max\{\sigma_1(v), \sigma_2(v), \ldots, \sigma_n(v)\}$, $M(\cdot)$ is the number of the maximum real part of eigenvalue less than zero in N times estimates. Moreover, the stochastic robust stability and stochastic robust performance can be introduced.

Similar to the definition of the instability probability, the probability that the dynamic out of performance envelope or the control variable saturated could be weighted summed to describe the performance of the closed-loop system. The sum is which named stochastic robustness cost function. When the structure of the controller has been chosen, the parameters of the controller can be designed by optimizing the cost function. The optimal control law from the point of stochastic robustness concepts is obtained.

For each performance demand, a two-valued indicator function is introduced to tell whether the closed-loop system satisfies this requirement in once simulation:

$$I[G(v), C(d)] = \begin{cases} 0, & \text{satified}, \\ 1, & \text{unsatified}, \end{cases} \quad v \in \mathcal{Q} \tag{49}$$

where d is the parameters to be designed, $\mathcal{Q}$ is the value set of uncertain parameters. Supposing that $f(v)$ is the combined probability density distribution function about v, the probability that closed-loop system violate this performance demand can be defined as follows [20]:

$$p = \int_{v\in\mathbb{Q}} I[G(v), C(d)]f(v)dv. \tag{50}$$

In practical application, this integral can be approximately calculated through Monte-Carlo simulation:

$$\hat{p} = \frac{1}{N}\sum_{k=1}^{N} I[H(v_k), G(d)] \tag{51}$$

where N is the simulation times, and $\hat{p}$ is the estimate of the violate probability.

Synthesize all the performance violate probability and instability probability, the stochastic robustness cost function can be defined as follows:

$$J(d) = \sum_{i=1}^{M} [w_i \hat{p}_i(d)] \tag{52}$$

where w_i is the weight, and M is the number of the indicators.

After the stochastic robustness cost function is defined, the last step is to use an optimization method to optimize this cost function. PIO algorithm introduced previously is applied in this optimization procedure. So far, the main principle of the stochastic robustness method has been presented.

V. Simulation Results and Analysis

In this section, the simulation results of the closed-loop system composed of the RLV and the controller designed by stochastic robustness design method are presented. Firstly, some simulation parameters setting are given out at the beginning of this section.

The test flight condition of the reusable launch vehicle is selected to give a design instance and evaluate the performance of the controller. This flight condition is selected refer to the flight envelope of the X-38. The flight condition selected is in Table I.

TABLE I
The Selected Flight Condition

h (m)	Ma	γ	$d\gamma/dt$	χ	$d\chi/dt$
30 000	2.8	−5	0	0	0

The evaluation commands are: angle of attack 5 degree step command, angle of side slip remains at the zero point, bank angle −5 degree step command.

The uncertainties of aerodynamic coefficients are supposed to subject to normal distribution, i.e.,:

$$v \sim \mathrm{N}(1, 0.15^2), \quad C_{ij} = vC_{ij} \tag{53}$$

where C_{ij} is the aerodynamic coefficients.

The design process goes for the different fractional order of the fractional SMC to give a preliminary study of the influence of the fractional orders. The parameters and performance indicators of stochastic robustness design method are set as in Table II, while the simulation times of Monte Carlo simulation $N = 50$.

The parameters to be optimized are the control parameters: $d = [k_w\ k_\alpha\ k_\beta\ k_\mu\ \sigma_\alpha\ \sigma_\beta\ \sigma_\mu\ \kappa_\alpha\ \kappa_\beta\ \kappa_\mu]^T$.

The parameters of PIO algorithm are set as follows: the number of pigeon $n = 20$, the map and compass operator $R = 0.02$, the iteration times of the map and compass operator $T_1 = 30$, the iteration times of landmark operator $T_2 = 5$.

Case 1: In this case, the stochastic robustness design for selected fractional order is focused on and the Monte-Carlo simulation is carried out to evaluate the designed parameters of the controller.

TABLE II
The Stability and Performance Metrics

Index	Weight	Indicator	Performance demand
1	8	I1	outputs convergence
2	0.1	I2	Regulation time at point 10% less than 1s
3	1	I3	Regulation time at point 10% less than 2s
4	1	I4	Overshoot less than 20%
5	0.1	I5	Overshoot less than 10%
6	1	I6	Deflection of aileron less than 40 deg
7	0.5	I7	Deflection of aileron less than 30 deg
8	1	I8	Deflection of elevator less than 40 deg
9	0.5	I9	Deflection of elevator less than 30 deg
10	1	I10	Deflection of rudder less than 40 deg
11	0.5	I11	Deflection of rudder less than 30 deg
12	1	I12	Deflection of body flap less than50 deg
13	0.5	I13	Deflection of body flap less than 40 deg

The fractional order of FSMC selected: $\lambda = -0.8, \eta = 0.9$. The result of design parameter is:

$$d = [1.8359\ \ 1.0651\ \ 2.1960\ \ 1.0364\ \ 3.4948 \times 10^{-5}\ \ 8.1261 \times 10^{-5}\ \ 6.2807 \times 10^{-5}\ \ 0.7458\ \ 1.2157\ \ 1.4024]$$

Fig. 2 shows the history of the stochastic robustness cost function in the design process based on PIO algorithm. Then the Monte-Carlo simulation goes for the closed loop system with the designed control parameters. Fig. 3 is the simulation results from which we can evaluate the robustness of the control system. The time history of attitude angles shows that they can steer the evaluation step command quickly and robustly though angle of attack has a tolerant steady-state error.

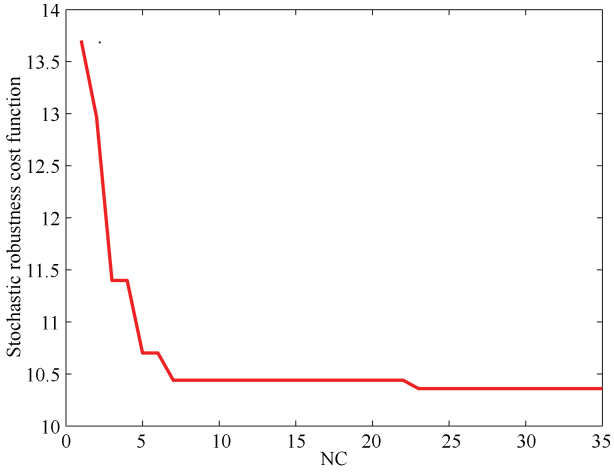

Fig. 2. The fitness value curve of PIO algorithm.

From the simulation results, the controller based on FSMC and DI can tolerate the uncertainties of aerodynamic parameters through the stochastic robustness design process.

Case 2: In this case, the design results based on stochastic robustness design method for the different fractional orders are compared, from which we can find out the influence of the fractional order in FSMC to the closed loop system.

Six groups of the fractional order are selected:

$$\begin{array}{llll} \lambda_1 = -1, & \eta_1 = 0.9; & \lambda_2 = -0.9, & \eta_2 = 0.9 \\ \lambda_3 = -0.8, & \eta_3 = 0.9; & \lambda_4 = -0.7, & \eta_4 = 0.9 \\ \lambda_5 = -0.7, & \eta_5 = 1; & \lambda_6 = -1, & \eta_6 = 1. \end{array}$$

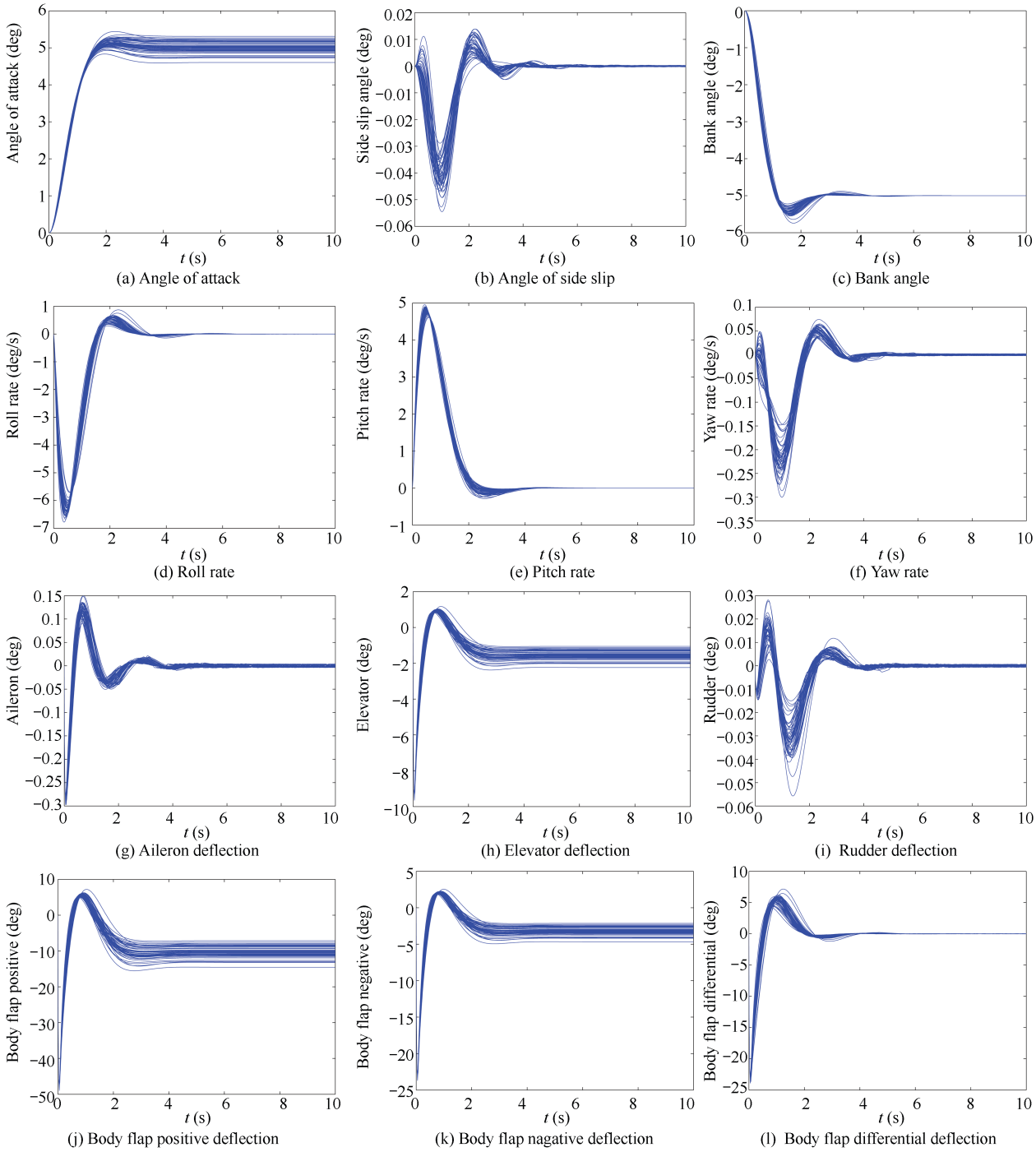

Fig. 3. Results of Monte Carlo simulation experiments.

These groups include different fractional order in the sliding surface function and fractional reaching law, as well as integral order sliding surface and reaching law. Through the stochastic robustness design procedure above, we obtain the optimal design parameters of the each controller with different fractional orders and integral order. The simulations of these closed-loop systems with different FSMC and SMC have been carried out. Fig. 4 gives the compared results of these closed-loop systems.

It should be noted that in these figures, symbol a represents the fractional integral order, while symbol b represents the fractional integral order. These compared results show how the different fractional orders in FSMC influence the performance of the closed loop system. For the group 1 to group 4, these groups all have the same fractional order of the reaching law and different fractional order of the sliding surface. The group 2 and group 3 have the similar performance, the response of the attitude angle is smoother and faster which means a shorter settling time and a smaller overshoot. Compared the control surface deflection, the group 2 and group 3 have a smaller control effectors but the group 1 and group 4 have one aerodynamic surface saturated. With the above factors combined, the group 2 and group 3 have more desirable performance. By Comparing the group 3 with the group 6

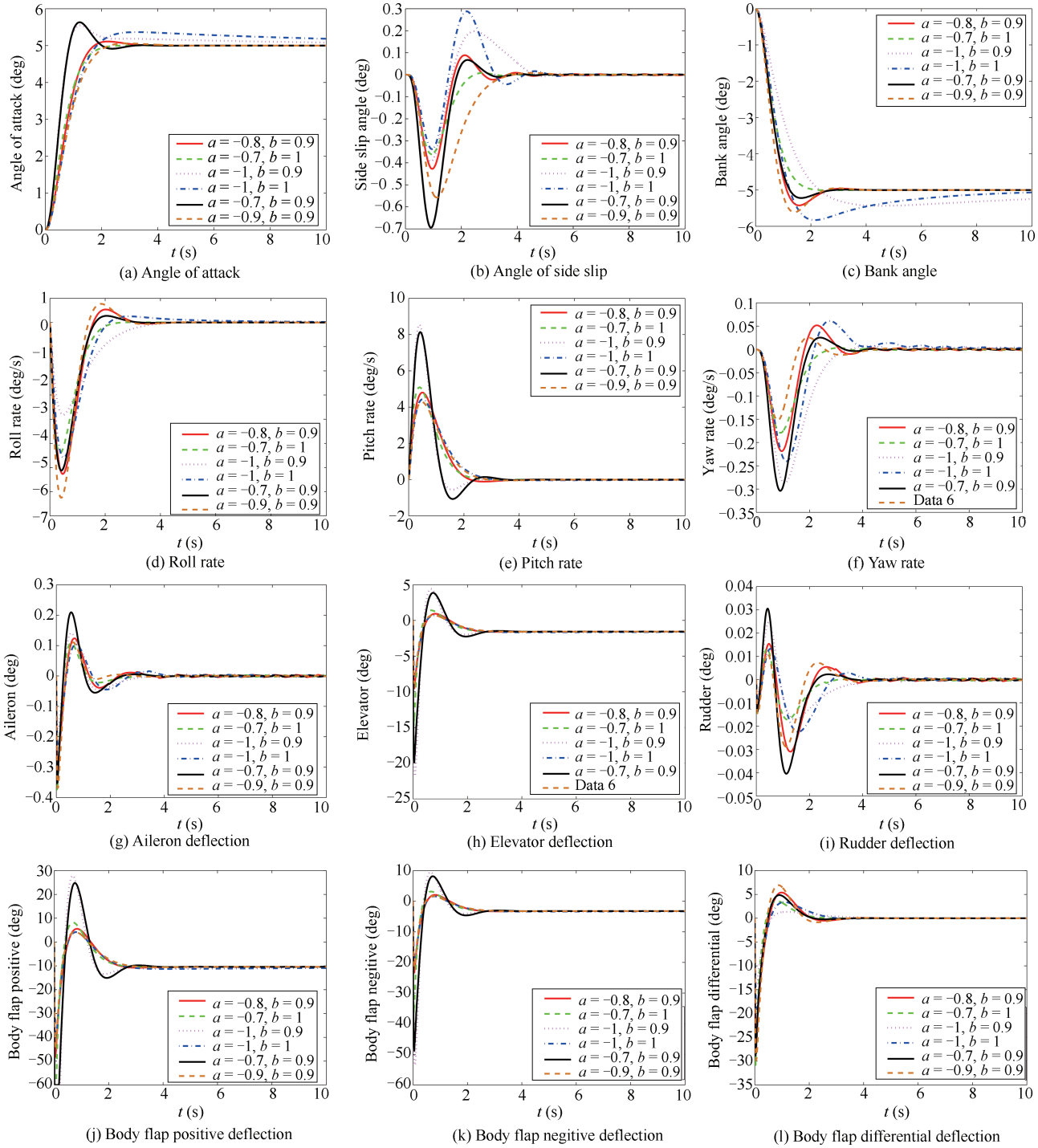

(a) Angle of attack (b) Angle of side slip (c) Bank angle

(d) Roll rate (e) Pitch rate (f) Yaw rate

(g) Aileron deflection (h) Elevator deflection (i) Rudder deflection

(j) Body flap positive deflection (k) Body flap negitive deflection (l) Body flap differential deflection

Fig. 4. Results of simulation experiments of different FSMC.

which has integral order sliding surface and reaching law, we can see that the attitude angle response of group 3 is smoother and faster than that of group 6. The control surface deflection in the group 6 is smaller than that in the group 3. Comparing the group 1, group 4, group 5 and group 6, we can see that the fractional order obviously influence the control variables. So the optimal fractional order or integral order in FSMC should been chosen by taking both the dynamic characters and control effects into count. In this study, the stochastic robustness design method for the different fractional orders also influence the performance of these controllers. The more credible mean to find the optimal fractional order in the controller remains a question.

VI. Conclusions

In this paper, we have established a robust controller for reusable launch vehicle based on fractional sliding mode technology and dynamic inversion approach. For the parameters of the controller, stochastic robustness design method based on PIO algorithm and Monte-Carlo simulations is applied to obtain the optimal values. The influence of different fractional order of the FSMC to the performance of closed loop system is discussed. The experimental results validate the effectiveness

and robustness of the combined robust controller when considering sufficient dispersion of aerodynamic coefficients. In addition, the fractional orders in sliding mode method improve the performance of the closed-loop system.

It should be pointed out that FSMCs with several different fractional orders in our control law are designed to compare the performance of the closed-loop systems. The direct analysis to obtain the optimal fractional order in FSMC for the closed-loop system has not been given out. In addition, how to simply the algorithm and make it more convenient in engineering is still a challenge. The more relative further work and details would be conducted in these issues in the future.

REFERENCES

[1] E. Mooij, "Aerospace-plane flight dynamics: analysis of guidance and control concepts," Ph.D. dissertation, Delft University of Technology, The Netherlands, 1998.

[2] A. J. Roenneke and K. H. Well, "Nonlinear flight control for a high-lift reentry vehicle," in *Guidance, Navigation, and Control Conf., Guidance, Navigation, and Control and Co-located Conf.*, Baltimore, MD, 1995, pp. 1798−1805.

[3] H. X. Wu and B. Meng, "Review on the control of hypersonic flight vehicles," *Adv. Mechan.*, vol. 39, no. 6, pp. 756−765, Nov. 2009.

[4] J. M. Hanson, "A plan for advanced guidance and control technology for 2nd generation reusable launch vehicles," in *AIAA Guidance, Navigation, and Control Conf. and Exhibit, Guidance, Navigation, and Control and Co-located Conf.* Monterey, California, USA, 2002, pp. 1−9.

[5] D. Ito, J. Georgie, J. Valasek, and D. T. Ward, "Reentry vehicle flight controls design guidelines: dynamic inversion," Technical Report NASA/TP-2002-210771, Mar. 1, 2002.

[6] C. Y. Wang, Y. Luo, and Y. Q. Chen, "An analytical design of fractional order proportional integral and [proportional integral] controllers for robust velocity servo," in *Proc. 4th IEEE Conf. Industrial Electronics and Applications (ICIEA 2009)*, Xi'an, China, 2009, pp. 3448−3453.

[7] B. C. Zhang, S. F. Wang, Z. P. Han, and C. M. Li, "Using fractional-order PID controller for control of aerodynamic missile," *J. Astronaut.*, vol. 26, no. 5, pp. 653−656, Sep. 2005.

[8] R. J. Adams, J. M. Buffington, and S. S. Banda, "Design of nonlinear control laws for high-angle-of-attack flight," *J. Guid. Contr. Dynam.*, vol. 17, no. 4, pp. 737−746, Jul. 1994.

[9] E. B. Jackson and C. I. Cruz, "Preliminary subsonic aerodynamic model for simulation studies of the HL-20 lifting body," Technical Report NASA TM-4302, Sep. 1992.

[10] E. B. Jackson, C. I. Cruz, and W. A. Ragsdale, "Real-time simulation model of the HL-20 lifting body," Technical Report NASA TM-107580, Aug. 1992.

[11] J. Reiner, G. J. Balas, and W. L. Garrard, "Flight control design using robust dynamic inversion and time-scale separation," *Automatica*, vol. 32, no. 11, pp. 1493−1504, Nov. 1996.

[12] I. Podlubny, "Fractional-order systems and $PI^{\lambda}D^{\mu}$-controllers," *IEEE Trans. Automat. Contr.*, vol. 44, no. 1, pp. 208−214, Jan. 1999.

[13] X. Yuan, H. Y. Zhang, and J. B. Yu, "Fractional-order derivative and design of fractional digital differentiators," *Acta Electron. Sin.*, vol. 32, no. 10, pp. 1658−1665, Oct. 2004.

[14] J. Y. Cao and B. G. Cao, "Digital realization and characteristics of fractional order controllers," *Contr. Theor. Appl.*, vol. 23, no. 5, pp. 791−799, Oct. 2006.

[15] W. T. Ma, Q. Z. Zhang, B. B. Shi, and C. Gao, "Robust control approach for re-entry vehicle based on inversion model," in *Proc. 29th Chinese Control Conf.*, Beijing, China, 2010, pp. 2005−2009.

[16] H. B. Duan and P. X. Qiao, "Pigeon-inspired optimization: a new swarm intelligence optimizer for air robot path planning," *Int. J. Intell. Comput. Cybernet.*, vol. 7, no. 1, pp. 24−37, Feb. 2014.

[17] H. B. Duan and X. H. Wang, "Echo state networks with orthogonal pigeon-inspired optimization for image restoration," *IEEE Trans. Neural Network. Learn. Syst.*, vol. 27, no. 11, pp. 2413−2425, Nov. 2016.

[18] H. B. Duan, H. X. Qiu, and Y. M. Fan, "Unmanned aerial vehicle close formation cooperative control based on predatory escaping pigeon-inspired optimization," *Sci. China Technol. Sci.*, vol. 45, no. 6, pp. 559−572, Apr. 2015.

[19] B. Zhang and H. B. Duan, "Three-dimensional path planning for uninhabited combat aerial vehicle based on predator-prey pigeon-inspired optimization in dynamic environment," *IEEE/ACM Trans. Computat. Biol. Bioinf.*, 2017, to be published, DOI:10.1109/TCBB.2015.2443789.

[20] L. R. Ray and R. F. Stengel, "Application of stochastic robustness to aircraft control systems," *J. Guid. Contr. Dynam.*, vol. 14, no. 6, pp. 1251−1259, Nov. 1991.

[21] C. I. Marrison and R. F. Stengel, "Design of robust control systems for a hypersonic aircraft," *J. Guid. Contr. Dynam.*, vol. 21, no. 1, pp. 58−63, Jan. 1998.

[22] Q. Wang and R. F. Stengel, "Robust nonlinear control of a hypersonic aircraft," *J. Guid. Contr. Dynam.*, vol. 23, no. 4, pp. 577−585, Jul. 2000.

[23] S. T. Wu, *Stochastic Robustness Analysis and Design for Guidance and Control System of Winged Missile*. Beijing: National Defense Industry Press, 2010.

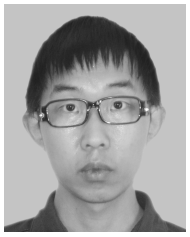

Qiang Xue is a master student at the School of Automation Science and Electrical Engineering, Beihang University, China. He received his bachelor degree from Beihang University in 2015. He is a member of BUAA Bio-inspired Autonomous Flight Systems (BAFS) Research Group. His reserach interests include multiple UAVs cooperative control and flight control.

Haibin Duan is a professor in the School of Automation Science and Electrical Engineering, Beihang University, China. He received his Ph.D. degree from Nanjing University of Aeronautics and Astronautics in 2005. He is the head of BUAA Bio-inspired Autonomous Flight Systems (BAFS) Research Group. His research interests include multiple UAVs cooperative control, biological computer vision and bio-inspired computation. Corresponding author of this paper.